Proceedings of the Eighteenth International Conference on
Civil, Structural and Environmental Engineering Computing
Edited by: P. Iványi, J. Kruis and B.H.V. Topping
Civil-Comp Conferences, Volume 10, Paper 8.3
Civil-Comp Press, Edinburgh, United Kingdom, 2025
ISSN: 2753-3239, doi: 10.4203/ccc.10.8.3

Mass Conservation for FSI Problems in Fictitious Domain Approach

F. Credali[1], N. Alshehri[1], D. Boffi[1,2] and L. Gastaldi[3]

[1] CEMSE Division, King Abdullah University of Science and Technology, Thuwal, Saudi Arabia
[2] Dipartimento di Matematica F. Casorati, Università degli Studi di Pavia, Italy
[3] Dipartimento di Ingegneria Civile, Architettura, Territorio, Ambiente e di Matematica (DICATAM), Università degli Studi di Brescia, Italy

Abstract

We consider the finite element discretization of a fictitious domain formulation for fluid-structure interaction problems where a distributed Lagrange multiplier is associated with the kinematic constraint. Fluid and solid equations are solved on independent meshes and a coupling term takes care of their interaction. In this work we discuss the mass conservation properties of several combinations of finite element spaces through some significant numerical tests.

Keywords: fluid-structure interactions, interface problems, fictitious domain method, Lagrange multiplier, unfitted finite elements, mass conservation.

1 Introduction

The scientific community has a large interest in developing effective numerical methods for the simulation of coupled and multiphysics problems such as fluid-structure

interactions, multiphase flows, and thermo-mechanical problems, since they have several engineering applications. We mention, for instance, cardiac mechanics, particulate flows and structural analysis.

The mathematical description of such problems usually couples partial differential equations of different kinds or involves discontinuous coefficients, hence the computational domain can be interpreted as the union of several regions with evolving interface. The numerical simulation of this class of problems is challenging from different points of view: for instance, a high resolution discretization of the geometry is required, and the governing equations may involve nonlinear terms.

During the last decades, a wide range of mathematical approaches have been presented to tackle the above problems and related issues. The Arbitrary Lagrangian–Eulerian approach [1, 2] employs meshes matching at the interface, so that kinematic constraints are satisfied by construction. Nevertheless, strong distortions and time instabilities may appear [3]. For these reasons, unfitted approaches gained popularity. Among them, we mention the immersed boundary method [4], the fictitious domain approach [5, 6], the level set method [7] and the Nitsche–XFEM [8].

Our distributed Lagrange multiplier formulation [9] originated from the immersed boundary method and then evolved towards a fictitious domain framework.

The aim of this work is to discuss the mass conservation properties of our method. It is well-known from the literature that standard finite element pairs for the incompressible Stokes equations (we mention, for instance, the Hood–Taylor [10], the Bercovier–Pironneau [11], and the MINI [12] elements) conserve mass only in an approximate sense since $\operatorname{div} \mathbf{V}_h \not\subset Q_h$. This argument is strictly connected with the *pressure robustness* property [13]: a finite element pair is pressure robust if the error committed on the velocity discretization is not affected by the pressure.

It is clear that the construction of conforming div-free finite element spaces is not trivial. We could resort to the finite element exterior calculus to design suitable spaces [14], or to Discontinuous Galerkin [15] and virtual element [16] methods, where the discrete divergence free property is ensured by construction of the spaces. All these techniques represent viable options, but they require additional effort when implementing the simulation methods.

There are at least two simple modifications that can be taken into account to improve the mass conservation of standard finite element pairs: the first one consists in adding the so-called *grad-div* stabilization [17], while the second one involves enriching continuous pressure spaces with an additional constant [18, 19]. Since the grad-div stabilization is an artificial penalty term, we decide for the second way. We already studied the effect of adding a constant to the pressure space in case of the Hood–Taylor and Bercovier–Pironneau elements [20].

After recalling the main features of our fictitious domain formulation, together with some computational aspects regarding its discretization in time and space, we compare and discuss the mass conservation properties of continuous and discontinuous finite element spaces for the pressure and the distributed Lagrange multiplier.

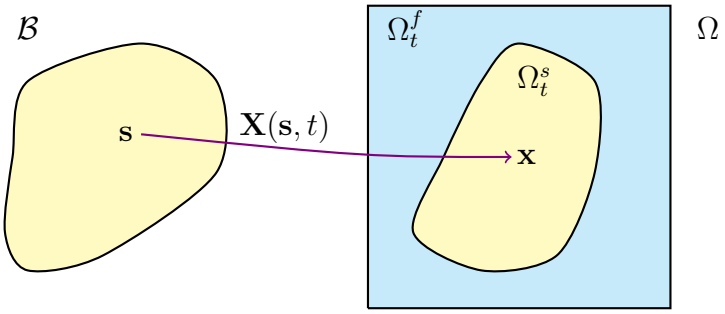

Figure 1: Example of geometric configuration. Ω and $\mathcal{B}$ are fixed domains, independent of time. The fluid dynamics is described with Eulerian coordinates. For the solid evolution, the Lagrangian framework is preferred: each point $\mathbf{s} \in \mathcal{B}$ is mapped into a point $\mathbf{x} \in \Omega_t^s$ through the map $\mathbf{X}$.

2 The continuous problem

We discuss the finite element discretization of fluid-structure interaction problems characterized by a thick visco-elastic solid body immersed in a Newtonian fluid. Both fluid and solid materials are incompressible.

The configuration of the system is described by two non-overlapping time dependent domains $\Omega_t^f, \Omega_t^s \subset \mathbb{R}^d$, $d = 2, 3$ representing the regions occupied by fluid and solid at time instant t, respectively. We assume that the region occupied by the union of fluid and solid regions does not depend on time. We then introduce the fixed domain $\Omega = \Omega_t^f \cup \Omega_t^s$ with the additional simplifying hypothesis that $\partial\Omega \cap \partial\Omega_t^s = \emptyset$. Even if our model can deal with more complex situations, we restrict ourselves to $d = 2$. An example of configuration for the FSI problem is sketched in Figure 1.

The fluid dynamics is governed by the Navier–Stokes equations described in Eulerian framework. Let $\mathbf{u}_f$ denote the fluid velocity and ρ_f the density, we have

$$\begin{aligned} \rho_f \dot{\mathbf{u}}_f &= \operatorname{div} \boldsymbol{\sigma}_f \quad \text{in } \Omega_t^f, \\ \operatorname{div} \mathbf{u}_f &= 0 \qquad \text{in } \Omega_t^f, \end{aligned} \tag{1}$$

where $\boldsymbol{\sigma}_f = -p_f \mathbb{I} + \nu_f \underline{\boldsymbol{\varepsilon}}(\mathbf{u}_f)$ is the Cauchy stress tensor for Newtonian fluids, which is expressed in terms of fluid pressure p_f, viscosity $\nu_f > 0$ and symmetric gradient of the velocity $\underline{\boldsymbol{\varepsilon}}(\mathbf{u}_f) = (\boldsymbol{\nabla}\, \mathbf{u}_f + (\boldsymbol{\nabla}\, \mathbf{u}_f)^\top)/2$. The second equation in (1) is the mass conservation equation and corresponds to the incompressibility property of the fluid.

On the other hand, the solid deformation is described in Lagrangian setting. We thus introduce a reference domain $\mathcal{B} \subset \mathbb{R}^d$ such that the actual configuration of the solid body Ω_t^s can be represented as a mapping of $\mathcal{B}$. Namely, we introduce the deformation function $\mathbf{X}(\cdot, t) : \mathcal{B} \to \Omega_t^s$ such that $\mathbf{x} = \mathbf{X}(\mathbf{s}, t)$ for $\mathbf{x} \in \Omega_t^s$ and $\mathbf{s} \in \mathcal{B}$. The solid material velocity $\mathbf{u}_s$ is then expressed in terms of $\mathbf{X}$ as

$$\mathbf{u}_s(\mathbf{x}, t) = \frac{\partial \mathbf{X}(\mathbf{s}, t)}{\partial t} \qquad \text{for } \mathbf{x} = \mathbf{X}(\mathbf{s}, t). \tag{2}$$

We recall that the solid body consists of incompressible visco-elastic material, thus $\operatorname{div} \mathbf{u}_s = 0$. Moreover, the associated Cauchy stress tensor $\boldsymbol{\sigma}_s$ takes into account both properties, that is $\boldsymbol{\sigma}_s = \boldsymbol{\sigma}_s^v + \boldsymbol{\sigma}_s^e$. More precisely, the viscous term is written as $\boldsymbol{\sigma}_s = -p_s \mathbb{I} + \nu_s \underline{\boldsymbol{\varepsilon}}(\mathbf{u}_s)$, where $\nu_s > 0$ denotes the solid viscosity and p_s is the Lagrange multiplier associated with the incompressibility. The elastic component $\boldsymbol{\sigma}_s^e$ is expressed by means of the first Piola–Kirchhoff elasticity tensor $\mathbb{P}$ through the following relation

$$\mathbb{P}(\mathbb{F}) = \mathcal{J}(\mathbf{s},t)\, \boldsymbol{\sigma}_s^e(\mathbf{x},t)\, \mathbb{F}^{-\top}(\mathbf{s},t) \qquad \text{for } \mathbf{x} = \mathbf{X}(\mathbf{s},t).$$

Here $\mathbb{F} = \boldsymbol{\nabla}_{\mathbf{s}} \mathbf{X}$ is the deformation gradient and $\mathcal{J}(\mathbf{s},t) = \det(\mathbb{F}(\mathbf{s},t))$. We obtain the following model for the solid

$$\begin{aligned} \rho_s \frac{\partial^2 \mathbf{X}}{\partial t^2} &= \operatorname{div}_{\mathbf{s}} \left(\mathcal{J} \boldsymbol{\sigma}_s^v \mathbb{F}^{-\top} + \mathbb{P}(\mathbb{F}) \right) && \text{in } \mathcal{B}, \\ \operatorname{div} \mathbf{u}_s &= 0 && \text{in } \Omega_t^s. \end{aligned} \tag{3}$$

Transmission conditions are considered to enforce continuity of velocity and Cauchy stress along the interface $\partial\Omega_t^s$, i.e.

$$\mathbf{u}_f = \mathbf{u}_s \qquad \text{and} \qquad \boldsymbol{\sigma}_f \mathbf{n}_f = -\left(\boldsymbol{\sigma}_s^v + \mathcal{J}^{-1} \mathbb{P}\mathbb{F}^{\top} \right) \mathbf{n}_s \qquad \text{on } \partial\Omega_t^s \cap \Omega_t^f, \tag{4}$$

where $\mathbf{n}_f$, $\mathbf{n}_s$ denote the outward unit normal vectors to fluid and solid domain, respectively. Finally, Equations (1), (3), (4) are completed by suitable initial conditions and by the no-slip condition for $\mathbf{u}_f$ on $\partial\Omega$

$$\begin{aligned} \mathbf{u}_f(0) &= \mathbf{u}_{f,0} && \text{in } \Omega_0^f, \\ \mathbf{u}_s(0) &= \mathbf{u}_{s,0} && \text{in } \Omega_0^s, \\ \mathbf{X}(0) &= \mathbf{X}_0 && \text{in } \mathcal{B}, \\ \mathbf{u}_f &= 0 && \text{on } \partial\Omega. \end{aligned}$$

We point out that the initial conditions $\mathbf{u}_{f,0} = \mathbf{u}_{s,0}$ on $\partial\Omega_0^s$.

In order to derive the variational fictitious domain formulation [9], we first extend the fluid domain Ω_t^f to the entire container Ω. Hence, we introduce the extended velocity $\mathbf{u}$ and pressure p defined as

$$\mathbf{u} = \begin{cases} \mathbf{u}_f & \text{in } \Omega_t^f \\ \mathbf{u}_s & \text{in } \Omega_t^s, \end{cases} \qquad p = \begin{cases} p_f & \text{in } \Omega_t^f \\ p_s & \text{in } \Omega_t^s. \end{cases}$$

We should take care of the motion of the immersed solid. Then, we impose that the material velocity of the solid is equal to the velocity $\mathbf{u}$ in the fictitious fluid, that is

$$\mathbf{u}(\mathbf{X}(\mathbf{s},t),t) = \frac{\partial \mathbf{X}(\mathbf{s},t)}{\partial t} \qquad \text{for } \mathbf{x} = \mathbf{X}(\mathbf{s},t). \tag{5}$$

We emphasize that this kinematic constraint is equivalent to (2) within the new framework. At variational level, (5) becomes

$$\mathbf{c}\left(\boldsymbol{\mu}, \mathbf{u}(\mathbf{X}(\mathbf{s},t),t) - \frac{\partial \mathbf{X}(\mathbf{s},t)}{\partial t} \right) = 0 \qquad \forall \boldsymbol{\mu} \in \boldsymbol{\Lambda},$$

where $\mathbf{\Lambda}$ is a suitable functional space and $\mathbf{c} : \mathbf{\Lambda} \times \mathbf{H}^1(\mathcal{B}) \to \mathbb{R}$ is a symmetric bilinear form such that $\mathbf{c}(\boldsymbol{\mu}, \mathbf{Z}) = 0 \; \forall \boldsymbol{\mu} \in \mathbf{\Lambda}$ implies $\mathbf{Z} = 0$ on $\mathcal{B}$.

The FSI problem in fictitious domain framework reads as follows.

Problem 1 *Given* $\mathbf{u}_0 \in \mathbf{H}^1_0(\Omega)$ *and* $\mathbf{X}_0 : \mathcal{B} \to \Omega$, $\forall t \in (0, T)$, *find* $\mathbf{u}(t) \in \mathbf{H}^1_0(\Omega)$, $p(t) \in L^2_0(\Omega)$, $\mathbf{X}(t) \in \mathbf{W}^{1,\infty}(\mathcal{B})$ *and* $\boldsymbol{\lambda}(t) \in \mathbf{\Lambda}$, *such that*

$$
\begin{aligned}
&\rho_f \left(\frac{\partial \mathbf{u}(t)}{\partial t}, \mathbf{v} \right)_\Omega + b(\mathbf{u}(t), \mathbf{u}(t), \mathbf{v}) + a(\mathbf{u}(t), \mathbf{v}) \\
&\qquad - (\operatorname{div} \mathbf{v}, p(t))_\Omega + \mathbf{c}(\boldsymbol{\lambda}(t), \mathbf{v}(\mathbf{X}(t))) = 0 \qquad && \forall \mathbf{v} \in \mathbf{H}^1_0(\Omega) \\
&(\operatorname{div} \mathbf{u}(t), q)_\Omega = 0 && \forall q \in L^2_0(\Omega) \\
&\delta\rho \left(\frac{\partial^2 \mathbf{X}}{\partial t^2}, \mathbf{Y} \right)_\mathcal{B} + (\mathbb{P}(\mathbb{F}(\mathbf{s}, t)), \boldsymbol{\nabla}_\mathrm{s} \mathbf{Y})_\mathcal{B} - \mathbf{c}(\boldsymbol{\lambda}(t), \mathbf{Y}) = 0 \qquad && \forall \mathbf{Y} \in \mathbf{H}^1(\mathcal{B}) \\
&\mathbf{c}\left(\boldsymbol{\mu}, \mathbf{u}(\mathbf{X}(\cdot, t), t) - \frac{\partial \mathbf{X}(\cdot, t)}{\partial t} \right) = 0 && \forall \boldsymbol{\mu} \in \mathbf{\Lambda} \\
&\mathbf{u}(\mathbf{x}, 0) = \mathbf{u}_0(\mathbf{x}) && \forall \mathbf{x} \in \Omega \\
&\mathbf{X}(\mathbf{s}, 0) = \mathbf{X}_0(\mathbf{s}) && \forall \mathbf{s} \in \mathcal{B}.
\end{aligned}
$$

The detailed derivation of Problem 1 can be found in [9]. In the above equations, $L^2_0(\Omega)$ stands for the subspace of $L^2(\Omega)$ containing null mean functions. Moreover, we adopted the notation $\delta\rho = \rho_s - \rho_f$ for the gap between solid and fluid density, while the forms $a(\cdot, \cdot)$ and $b(\cdot, \cdot, \cdot)$ represent diffusion and convection in the fluid domain, respectively,

$$
a(\mathbf{u}, \mathbf{v}) = (\nu \, \underline{\boldsymbol{\varepsilon}}(\mathbf{u}), \underline{\boldsymbol{\varepsilon}}(\mathbf{v}))_\Omega \,, \qquad b(\mathbf{u}, \mathbf{v}, \mathbf{w}) = \frac{\rho_f}{2} \left((\mathbf{u} \cdot \nabla \mathbf{v}, \mathbf{w})_\Omega - (\mathbf{u} \cdot \nabla \mathbf{w}, \mathbf{v})_\Omega \right).
$$

We observe that the viscosity ν takes value ν_s in Ω^s_t and ν_f in Ω^f_t. We define the space $\mathbf{\Lambda} = (\mathbf{H}^1(\mathcal{B}))'$ as the dual space of $\mathbf{H}^1(\mathcal{B})$, and the coupling term $\mathbf{c}(\cdot, \cdot)$ as

$$
\mathbf{c}(\boldsymbol{\mu}, \mathbf{Z}) = \langle \boldsymbol{\mu}, \mathbf{Z} \rangle \quad \forall \boldsymbol{\mu} \in \mathbf{\Lambda}, \; \mathbf{Z} \in \mathbf{H}^1(\mathcal{B})
$$

with $\langle \cdot, \cdot \rangle$ being the duality pairing between $\mathbf{H}^1(\mathcal{B})$ and $\mathbf{\Lambda}$.

3 Discretization

In this section we describe the discretization of Problem 1 in time and space.

Concerning the time discretization, we consider the Backward Euler scheme on a uniform partition $\{t_n = n\Delta t\}_{n=0}^N$ of the time interval $[0, T]$.

The space discretization is carried out by mixed finite elements. Let $\mathcal{T}^\Omega_h$ be a triangulation of the fluid domain Ω having size h_Ω, and let $\mathcal{T}^\mathcal{B}_h$ be a triangular mesh of the solid reference domain $\mathcal{B}$ with size $h_\mathcal{B}$. We introduce four finite dimensional subspaces: $\mathbf{V}_h \subset \mathbf{H}^1_0(\Omega)$, $Q_h \subset L^2_0(\Omega)$, $\mathbf{S}_h \subset \mathbf{H}^1(\mathcal{B})$ and $\mathbf{\Lambda}_h \subset \mathbf{\Lambda}$. More precisely, $\mathbf{V}_h$

and Q_h are the discrete spaces for the velocity $\mathbf{u}$ and the pressure p, respectively, and must satisfy the discrete inf-sup conditions prescribed for the Stokes problem. On the other hand, $\mathbf{S}_h$ is the discrete space in which we solve the solid unknown $\mathbf{X}$ and $\mathbf{\Lambda}_h$ is the space for the discrete Lagrange multiplier.

Remark 1 *At the discrete level, we identify the duality pairing between* $\mathbf{H}^1(\mathcal{B})$ *and its dual by the scalar product in* $\mathbf{L}^2(\mathcal{B})$ *since* $\mathbf{\Lambda}_h \subset \mathbf{L}^2(\mathcal{B})$*. As a consequence, the coupling term is defined as* $\mathbf{c}(\boldsymbol{\mu}_h, \mathbf{Y}_h) = (\boldsymbol{\mu}_h, \mathbf{Y}_h)_{\mathcal{B}}$ *for all* $\boldsymbol{\mu}_h \in \mathbf{\Lambda}_h$ *and* $\mathbf{Y}_h \in \mathbf{S}_h$*.*

The fully discrete version of Problem 1 reads as follows.

Problem 2 *Given* $\mathbf{u}_h^0 \in \mathbf{V}_h$ *and* $\mathbf{X}_h^0 \in \mathbf{S}_h$*, for* $n = 1, \dots, N$ *find* $\mathbf{u}_h^n \in \mathbf{V}_h$*,* $p_h^n \in Q_h$*,* $\mathbf{X}_h^n \in \mathbf{S}_h$*, and* $\boldsymbol{\lambda}_h^n \in \mathbf{\Lambda}_h$*, such that*

$$
\begin{aligned}
&\rho_f\left(\frac{\mathbf{u}_h^{n+1}-\mathbf{u}_h^n}{\Delta t}, \mathbf{v}\right) + b(\mathbf{u}_h^n, \mathbf{u}_h^{n+1}, \mathbf{v}_h) + a(\mathbf{u}_h^{n+1}, \mathbf{v}_h) \\
&\qquad\qquad - (\operatorname{div}\mathbf{v}_h, p_h^{n+1}) + (\boldsymbol{\lambda}_h^{n+1}, \mathbf{v}_h(\mathbf{X}_h^n))_{\mathcal{B}} = 0 \quad \forall \mathbf{v}_h \in \mathbf{V}_h \\
&(\operatorname{div}\mathbf{u}_h^{n+1}, q_h) = 0 \qquad\qquad \forall q_h \in Q_h \\
&\delta\rho\left(\frac{\mathbf{X}_h^{n+1}-2\mathbf{X}_h^n+\mathbf{X}_h^{n-1}}{\Delta t^2}, \mathbf{Y}_h\right)_{\mathcal{B}} + (\mathbb{P}(\mathbb{F}^{n+1}), \boldsymbol{\nabla}_{\mathrm{s}}\mathbf{Y}_h)_{\mathcal{B}} \\
&\qquad\qquad - (\boldsymbol{\lambda}_h^{n+1}, \mathbf{Y}_h)_{\mathcal{B}} = 0 \quad \forall \mathbf{Y}_h \in \mathbf{S}_h \\
&\left(\boldsymbol{\mu}_h, \mathbf{u}_h^{n+1}(\mathbf{X}_h^n) - \frac{\mathbf{X}_h^{n+1}-\mathbf{X}_h^n}{\Delta t}\right)_{\mathcal{B}} = 0 \qquad \forall \boldsymbol{\mu}_h \in \mathbf{\Lambda}_h.
\end{aligned}
$$

In order to initialize the advancing scheme, the term $\mathbf{X}_h^{-1}$ can be computed from the initial condition $\mathbf{u}_0$ as the solution of

$$
\mathbf{u}_0 = \frac{\mathbf{X}_h^0 - \mathbf{X}_h^{-1}}{\Delta t} \qquad \text{in } \mathcal{B}.
$$

We point out that the nonlinear term $b(\mathbf{u}_h^n, \mathbf{u}_h^{n+1}, \mathbf{v}_h)$, as well as the coupling terms $(\boldsymbol{\lambda}_h^{n+1}, \mathbf{v}_h(\mathbf{X}_h^n))_{\mathcal{B}}$ and $(\boldsymbol{\mu}_h, \mathbf{u}_h^{n+1}(\mathbf{X}_h^n))_{\mathcal{B}}$, are treated semi-implicitly. In the former case, we plug $\mathbf{u}_h^n$ in $b(\cdot,\cdot,\cdot)$, while in the latter we take into account the position of the immersed body at the previous time instant through the composition of $\mathbf{u}_h$ and $\mathbf{v}_h$ with the mapping $\mathbf{X}_h^n$. This semi-implicit time stepping scheme is unconditionally stable [9, Prop. 3], that is no requirements are prescribed on the choice of the time step Δt.

The term $\mathbb{P}(\mathbb{F}^{n+1})$ with $\mathbb{F}^{n+1} = \boldsymbol{\nabla}_{\mathrm{s}}\mathbf{X}_h^{n+1}$, which represents the elastic properties of the solid material, may also be nonlinear. In this case, additional linearization techniques can be considered depending on the chosen constitutive law or nonlinear solvers, such as the Newton and fixed point methods, can be employed for solving the equations. Since more general models are not the main object of this investigation, we will only consider the generalized neo–Hookean linear model, that is $\mathbb{P}(\mathbb{F}^{n+1}) = \kappa\,\mathbb{F}^{n+1}$, where κ is a positive constant.

The assembly of the finite element matrix associated with coupling terms like $(\boldsymbol{\mu}_h, \mathbf{v}_h(\mathbf{X}_h^n))_{\mathcal{B}}$ is challenging since it requires the integration of functions defined over grids independent of each other. Indeed, $\boldsymbol{\mu}_h \in \boldsymbol{\Lambda}_h$ is defined on the solid reference mesh $\mathcal{T}_h^{\mathcal{B}}$, whereas $\mathbf{v}_h \in \mathbf{V}_h$ is constructed on $\mathcal{T}_h^{\Omega}$. Moreover, the composition of $\mathbf{v}_h$ with the mapping $\mathbf{X}_h^n$ takes care of the actual position of the solid body. We discussed computational and theoretical aspects regarding this procedure in [21, 22]. In particular, we can either compute exactly such terms by implementing a composite quadrature rule on the intersection between the image of $\mathcal{T}_h^{\mathcal{B}}$ through $\mathbf{X}$ and the background mesh $\mathcal{T}_h^{\Omega}$ or, alternatively, we can skip the computation of the intersection and take into account the presence of a quadrature error. In this work we compute the coupling terms by means of the exact procedure.

We discretize the fluid sub-problem by the Bercovier–Pironneau element [11]: for the velocity, we consider the $\mathsf{P}_1 iso \mathsf{P}_2$ space, which mimics a quadratic approximation by employing piecewise linear elements, while for the pressure we consider both the standard continuous piecewise linear element P_1 and its enhanced version $\mathsf{P}_1 + \mathsf{P}_0$. For the solid deformation, we choose again the P_1 element.

As mentioned in the introduction, we work with both continuous [23] and discontinuous Lagrange multiplier spaces [24], and study their effect in terms of mass conservation. The choice of a discontinuous $\boldsymbol{\Lambda}_h$ is admissible since the coupling form is the scalar product in $\mathbf{L}^2(\mathcal{B})$.

Here is a summary of all the finite elements combinations we are going to use for our numerical tests:

- **Element 1:** $\mathsf{P}_1 iso \mathsf{P}_2 - \mathsf{P}_1 - \mathsf{P}_1 - \mathsf{P}_1$,
- **Element 2:** $\mathsf{P}_1 iso \mathsf{P}_2 - (\mathsf{P}_1 + \mathsf{P}_0) - \mathsf{P}_1 - \mathsf{P}_1$,
- **Element 3:** $\mathsf{P}_1 iso \mathsf{P}_2 - \mathsf{P}_1 - (\mathsf{P}_1 + \mathsf{B}_3) - \mathsf{P}_0$,
- **Element 4:** $\mathsf{P}_1 iso \mathsf{P}_2 - (\mathsf{P}_1 + \mathsf{P}_0) - (\mathsf{P}_1 + \mathsf{B}_3) - \mathsf{P}_0$.

We observe that, when a piecewise constant element is considered for the Lagrange multiplier, the solid space $\mathbf{S}_h$ must be enriched by the space B_3 of local cubic bubbles vanishing at the boundary of each element. This enrichment is required to ensure the stability of the discrete scheme [24].

4 Numerical tests

In this section we present two numerical tests to discuss the mass conservation properties of Elements 1–4.

4.1 Stationary problem: the circle

We first consider a steady-state version of Problem 2 to study the convergence of the method with respect to $h-$refinement. The fluid domain Ω is the unit square, while

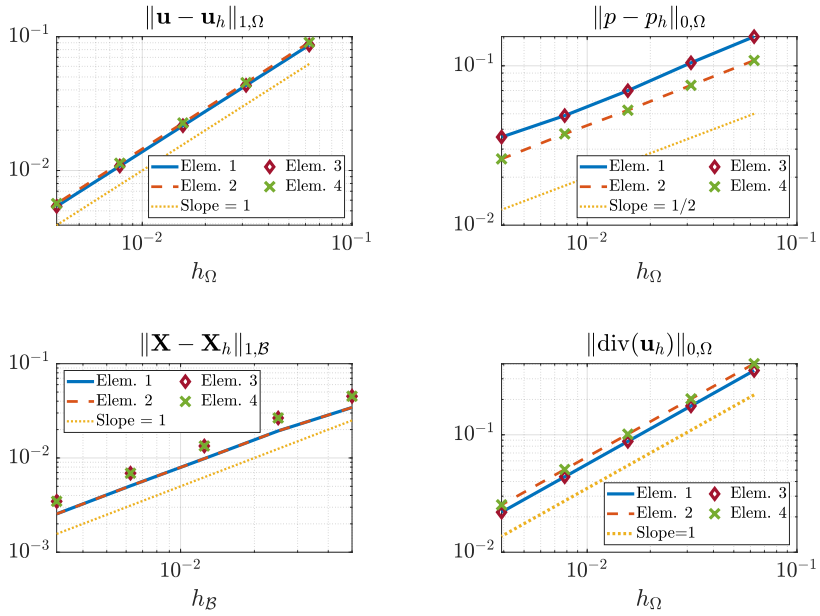

Figure 2: Convergence plots for the immersed circle (stationary case).

the immersed solid is the circle $\mathcal{C}_r$ with radius $r = 0.2$ and center at $(0.5, 0.5)$. The reference and actual configurations of the solid body coincide, that is $\mathcal{B} = \Omega_0^s$. The fluid dynamics is governed by the Stokes equations, while the solid is made of linear elastic material with coefficient $\kappa = 1$. We set the right hand side in such a way that the following solution is obtained:

$$
\begin{aligned}
&u_1(x,y) = 2x^2y(x-1)^2(y-1)^2 + x^2y^2(2y-2)(x-1)^2,\\
&u_2(x,y) = -2xy^2(x-1)^2(y-1)^2 - x^2y^2(2x-2)(y-1)^2,\\
&p = \begin{cases} \sin(\pi x)\sin(\pi y) - \frac{4}{\pi^2} + \frac{1}{2} & \text{in } \Omega^s \\ \sin(\pi x)\sin(\pi y) - \frac{4}{\pi^2} - \frac{\pi}{2(25-\pi)} & \text{in } \Omega^f, \end{cases}\\
&\mathbf{X}(s_1,s_2) = \left(s_1^4 - 2s_1^3 + s_1^2, -2s_2^3 + 3s_2^2 - s_2\right),\\
&\boldsymbol{\lambda}(s_1,s_2) = \left(s_2\sin(s_1), s_2\cos(s_1)\right),
\end{aligned}
\tag{6}
$$

where $\mathbf{x} = (x, y) \in \Omega$ and $\mathbf{s} = (s_1, s_2) \in \mathcal{B}$.

Convergence plots for $\mathbf{u}$, p, $\mathbf{X}$ and $\mathrm{div}(\mathbf{u})$ are collected in Figure 2. We observe that all errors decay with the expected rate, that is 1 for $\mathbf{u}$, $\mathbf{X}$, $\mathrm{div}(\mathbf{u})$ and 1/2 for the pressure due to its singularity at the interface. The choice of a discountinous pressure space (Elements 2 and 4) slightly improves the error of the pressure, while the error of the deformation $\mathbf{X}$ is rather better when the Lagrange multiplier is continuous (Elements 1 and 2).

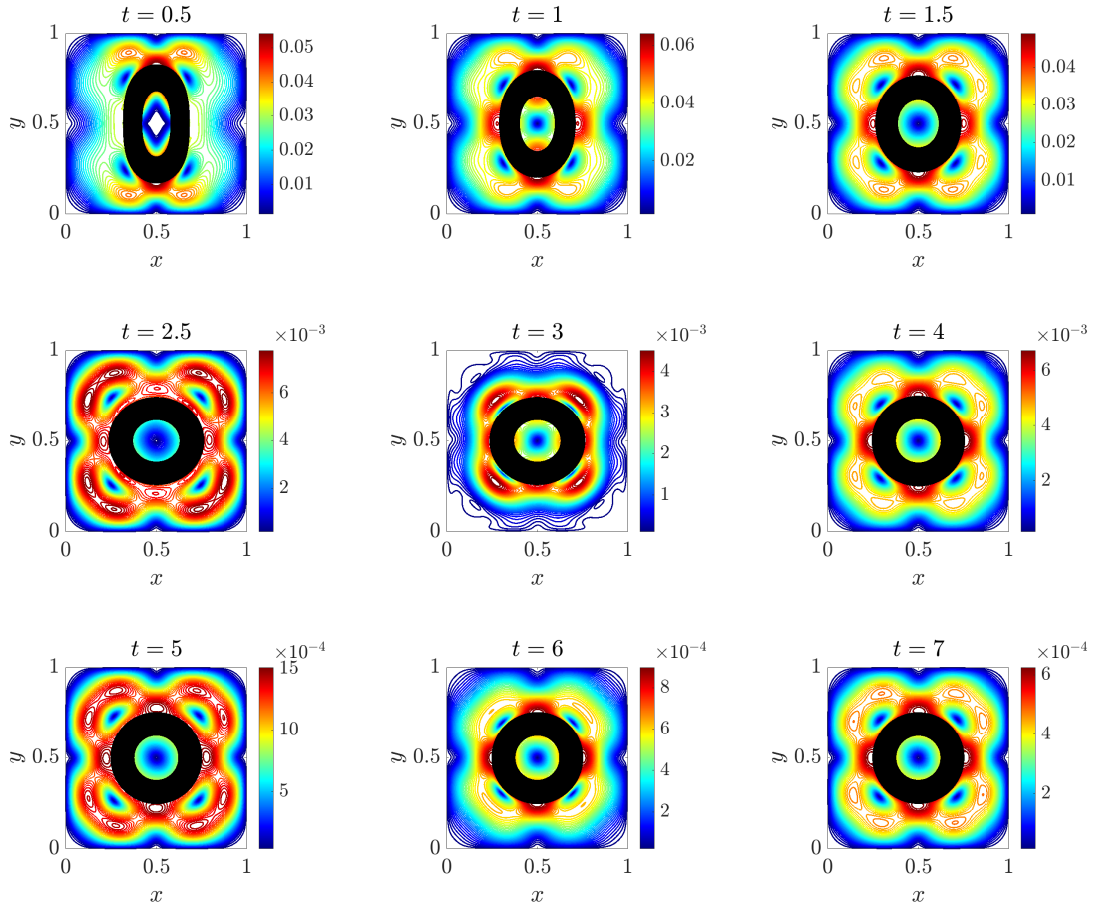

Figure 3: Velocity streamlines and evolution of the annulus.

4.2 Time dependent problem: the annulus

We then consider a time dependent problem to study the mass conservation. The fluid dynamics is governed by the Navier–Stokes equations in $\Omega = [0,1]^2$. The immersed solid is a linear elastic annulus centered at $(0.5, 0.5)$ and having elasticity parameter $\kappa = 0.2$. The solid reference domain corresponds to the annulus at rest, i.e. $\mathcal{B} = \{\mathbf{s} \in \mathbb{R}^2 : 0.125 \leq |\mathbf{s}| \leq 0.25\}$. Fluid and solid materials have the same viscosity $\nu = 0.01$, but different densities $\rho_f = 1.0$, $\rho_s = 1.1$.

At the beginning of the simulation, the fluid is stationary ($\mathbf{u}_0 = 0$), while the annulus is stretched with initial deformation given by $\mathbf{X}_0 = \left(\frac{s_1}{1.4}, 1.4\, s_2\right)$. The internal elastic forces make the annulus returning to its resting configuration, which originates the motion of the fluid.

We study the evolution of the system in the time interval $[0, 7]$ by choosing $\Delta t = 0.1$ and $\Delta t = 0.01$. Moreover, three spatial resolutions are considered: coarse test ($h_\Omega = 1/32$, $h_\mathcal{B} \approx 1/16$), medium test ($h_\Omega = 1/64$, $h_\mathcal{B} \approx 1/32$), and fine test ($h_\Omega = 1/128$, $h_\mathcal{B} \approx 1/64$). Some snapshots are collected in Figure 3 for $\Delta t = 0.01$, $h_\Omega = 1/128$, $h_\mathcal{B} \approx 1/64$ and Element 2.

In Figure 4, mass conservation is studied by measuring the relative volume change $1 - |\Omega_t^s|/|\Omega_0^s|$, where $|\Omega_t^s|$ denotes the area of the solid at the time instant t. In general, the larger area variation happens during the initial phase of the simulation ($t \leq 3$), in correspondence of larger solid deformations. From the plots, it is clear that Element 2 provides better conservation properties than the other elements: indeed, for Element 2, the maximum variation is less than $5 \times 10^{-3}\%$, whereas for Elements 1, 3, 4 the variation is around $5 \times 10^{-2}\%$. We observe that the behavior does not change when meshes are refined. We also highlight that the choice of a discontinuous Lagrange multiplier space $\mathbf{\Lambda}_h$ (Elements 3, 4) does not improve mass conservation. Thus, in agreement with [20], only a discontinuous pressure element gives better conservation. A detailed analysis of Element 2 is reported in Figure 5: when $\Delta t = 0.1$, the volume change is less than $4 \times 10^{-3}\%$, while for $\Delta t = 0.01$, it is less then $1 \times 10^{-3}\%$. Thus, the mass conservation is strictly related to the choice of time step.

We also analyze the behavior of $\mathrm{div}(\mathbf{u}_h)$ by computing its L^2-norm in time, as reported in Figure 6. Clearly, $\|\mathrm{div}(\mathbf{u}_h)\|_{0,\Omega}$ slightly reduces when refining the meshes. We notice that, for all the three geometric resolutions, Elements 2 and 4 perform better since the maximum value reached by $\|\mathrm{div}(\mathbf{u}_h)\|_{0,\Omega}$ is half than the maximum value obtained for Elements 1 and 3. This fact is clearer by looking at Figure 7. Elements 2 and 4 provide equivalent results thanks to the fact that the pressure is discontinuous.

5 Concluding remarks

We considered a fictitious domain formulation for fluid-structure interaction problems. Fluid and solid equations are solved on two independent meshes and a distributed Lagrange multiplier is responsible for their coupling.

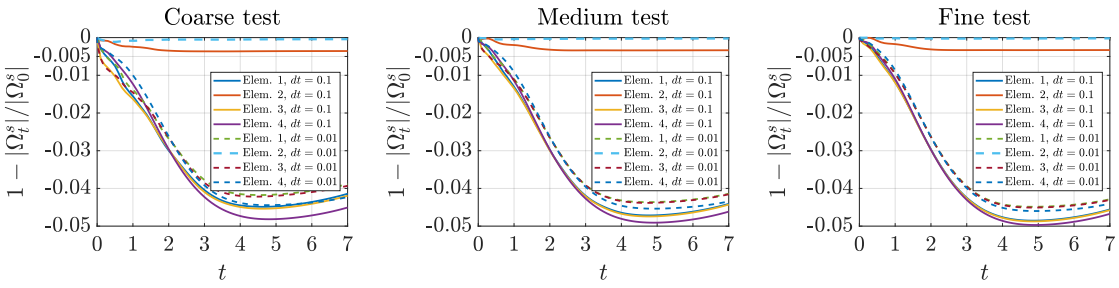

Figure 4: Volume change of the immersed annulus during the evolution of the system. Comparison of Elements 1–4 for three different geometric resolutions and time step $\Delta t = 0.1$ (solid lines), $\Delta t = 0.01$ (dashed lines).

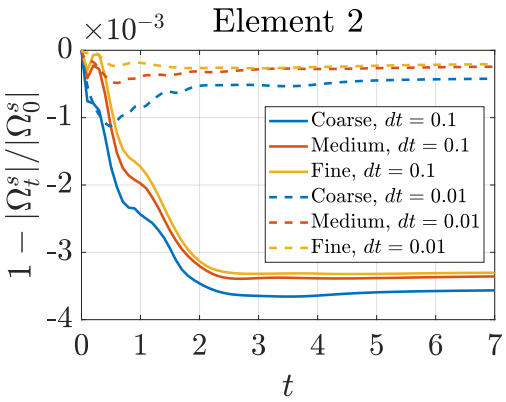

Figure 5: Volume change for Element 2 for the three mesh resolutions and time step $\Delta t = 0.1$ (solid lines) and $\Delta t = 0.01$ (dashed lines).

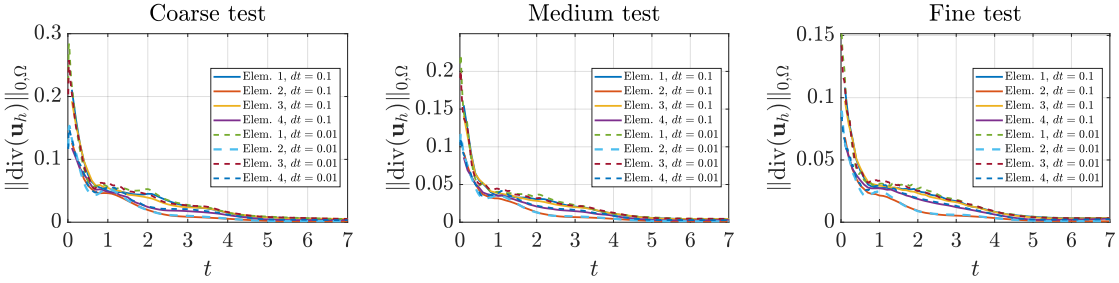

Figure 6: Norm of $\mathrm{div}\,\mathbf{u}_h(t)$ during the evolution of the annulus system. Comparison of Elements 1–4 for three different geometric resolutions and time step $\Delta t = 0.1$ (solid lines), $\Delta t = 0.01$ (dashed lines).

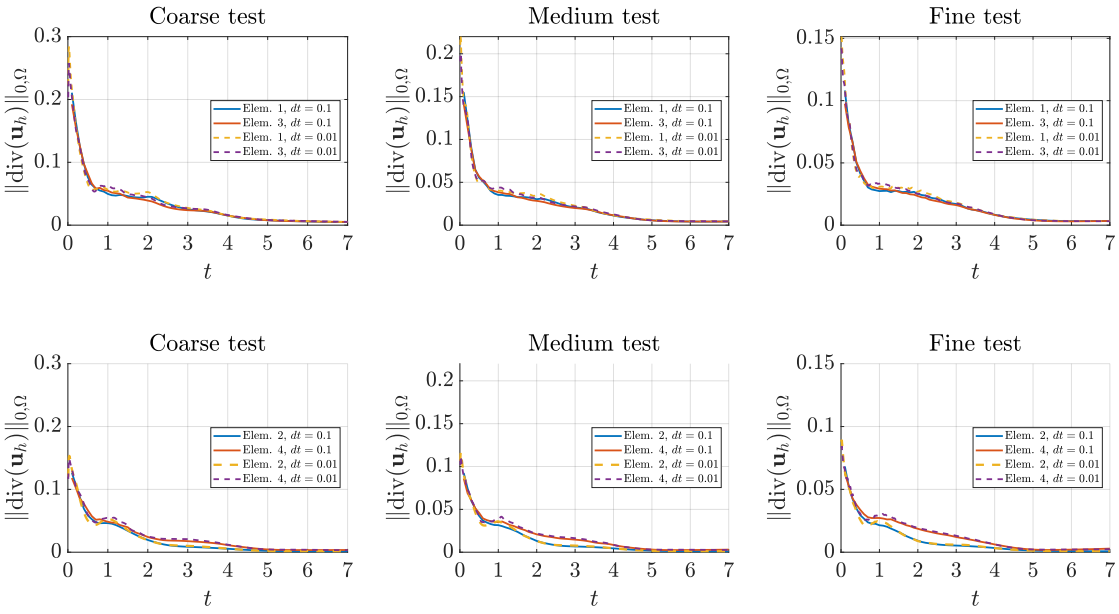

Figure 7: Detail of Figure 6, norm of $\mathrm{div}\,\mathbf{u}_h(t)$ during the evolution of the annulus system for $\Delta t = 0.1$ (solid lines) and $\Delta t = 0.01$ (dashed lines). Top line: Elements 1, 3 (continuous pressure elements), Elements 2, 4 (discontinuous pressure elements).

We focused on the finite element discretization and we discussed mass conservation properties of our formulation.

After recalling that popular finite element pairs for the Stokes equations are not divergence-free, we considered four different combinations of elements with continuous and discontinuous spaces for pressure and Lagrange multiplier.

Our numerical investigation confirmed that the choice of a discontinuous pressure space improves both mass conservation and divergence-free properties of the Bercovier–Pironneau element. A discontinuous multiplier space does not give a clear improvement in this regard, but this may be due to our specific choice of Stokes elements. Further investigation will focus on different types of finite element spaces, by considering both divergence free and higher order discretizations.

Acknowledgements

D. Boffi, F. Credali and L. Gastaldi are members of GNCS/INdAM Research group.
L. Gastaldi is partially supported by PRIN/MUR (Grant 20227K44ME) and IMATI/CNR.

References

[1] C. W. Hirt, A. A. Amsden, and J. L. Cook, “An arbitrary Lagrangian-Eulerian computing method for all flow speeds”, Journal of Computational Physics 14.3

(1974): 227-253.

[2] J. Donea, S. H. J. P. Giuliani, and J. P. Halleux, "An arbitrary Lagrangian–Eulerian finite element method for transient dynamic fluid-structure interactions", Computer Methods in Applied Mechanics and Engineering 33.1-3 (1982): 689-723.

[3] P. Causin, J. F. Gerbeau, and F. Nobile, "Added-mass effect in the design of partitioned algorithms for fluid-structure problems", Computer Methods in Applied Mechanics and Engineering 194.42-44 (2005): 4506-4527.

[4] C. S. Peskin, "The immersed boundary method", Acta Numerica 11 (2002): 479-517.

[5] R. Glowinski, T. W. Pan, and J. Periaux, "A Lagrange multiplier/fictitious domain method for the numerical simulation of incompressible viscous flow around moving rigid bodies:(I) case where the rigid body motions are known a priori", Comptes Rendus de l'Académie des Sciences-Series I-Mathematics 324.3 (1997): 361-369.

[6] R. Glowinski, T. W. Pan, T. I. Hesla, D. D. Joseph, and J. Periaux, "A fictitious domain approach to the direct numerical simulation of incompressible viscous flow past moving rigid bodies: application to particulate flow", Journal of Computational Physics 169.2 (2001): 363-426.

[7] M. Sussman, P. Smereka, and S. Osher, "A level set approach for computing solutions to incompressible two-phase flow", Journal of Computational Physics 114.1 (1994): 146-159.

[8] F. Alauzet, B. Fabrèges, M. A. Fernández, and M. Landajuela, "Nitsche–XFEM for the coupling of an incompressible fluid with immersed thin-walled structures", Computer Methods in Applied Mechanics and Engineering 301 (2016): 300-335.

[9] D. Boffi, N. Cavallini, and L. Gastaldi, "The finite element immersed boundary method with distributed Lagrange multiplier", SIAM Journal on Numerical Analysis 53.6 (2015): 2584-2604.

[10] P. Hood, and C. Taylor, "Navier-Stokes equations using mixed interpolation", Finite element methods in flow problems (1974): 121-132.

[11] M. Bercovier, and O. Pironneau, "Error estimates for finite element method solution of the Stokes problem in the primitive variables", Numerische Mathematik 33 (1979): 211-224.

[12] D. N. Arnold, F. Brezzi, and M. Fortin, "A stable finite element for the Stokes equations", Calcolo 21.4 (1984): 337-344.

[13] V. John, A. Linke, C. Merdon, M. Neilan, and L. G. Rebholz, "On the divergence constraint in mixed finite element methods for incompressible flows", SIAM review 59.3 (2017): 492-544.

[14] D. N. Arnold, R. S. Falk, and R. Winther, "Finite element exterior calculus, homological techniques, and applications", Acta Numerica 15 (2006): 1-155.

[15] B. Cockburn, G. Kanschat, and D. Schotzau, "A note on discontinuous Galerkin divergence-free solutions of the Navier–Stokes equations", Journal of Scientific Computing 31 (2007): 61-73.

[16] L. Beirão da Veiga, F. Brezzi, L. D. Marini, and A. Russo, "The virtual element method", Acta Numerica 32 (2023): 123-202.
[17] M. Olshanskii, and A. Reusken, "Grad-div stabilization for Stokes equations", Mathematics of Computation 73.248 (2004): 1699-1718.
[18] P. M. Gresho , R. L. Lee, S. T. Chan, and J. M. Leone Jr, "New finite element for Boussinesq fluids", No. UCRL-82842; CONF-800613-1. California Univ., Livermore (USA). Lawrence Livermore Lab., 1979.
[19] D. F. Griffiths, "The effect of pressure approximations on finite element calculations of incompressible flows", Department of Mathematical Sciences, University of Dundee, 1982.
[20] D. Boffi, N. Cavallini, F. Gardini, and L. Gastaldi, "Local mass conservation of Stokes finite elements", Journal of scientific computing 52 (2012): 383-400.
[21] D. Boffi, F. Credali, and L. Gastaldi, "On the interface matrix for fluid–structure interaction problems with fictitious domain approach", Computer Methods in Applied Mechanics and Engineering 401 (2022): 115650.
[22] D. Boffi, F. Credali, and L. Gastaldi, "Quadrature error estimates on non-matching grids in a fictitious domain framework for fluid-structure interaction problems", arXiv preprint arXiv:2406.03981 (2024).
[23] D. Boffi and L. Gastaldi, "A fictitious domain approach with Lagrange multiplier for fluid-structure interactions", Numerische Mathematik 135 (2017): 711-732.
[24] N. Alshehri, D. Boffi, and L. Gastaldi, "Unfitted mixed finite element methods for elliptic interface problems", Numerical Methods for Partial Differential Equations 40.1 (2024): e23063.